

# RSC Advances

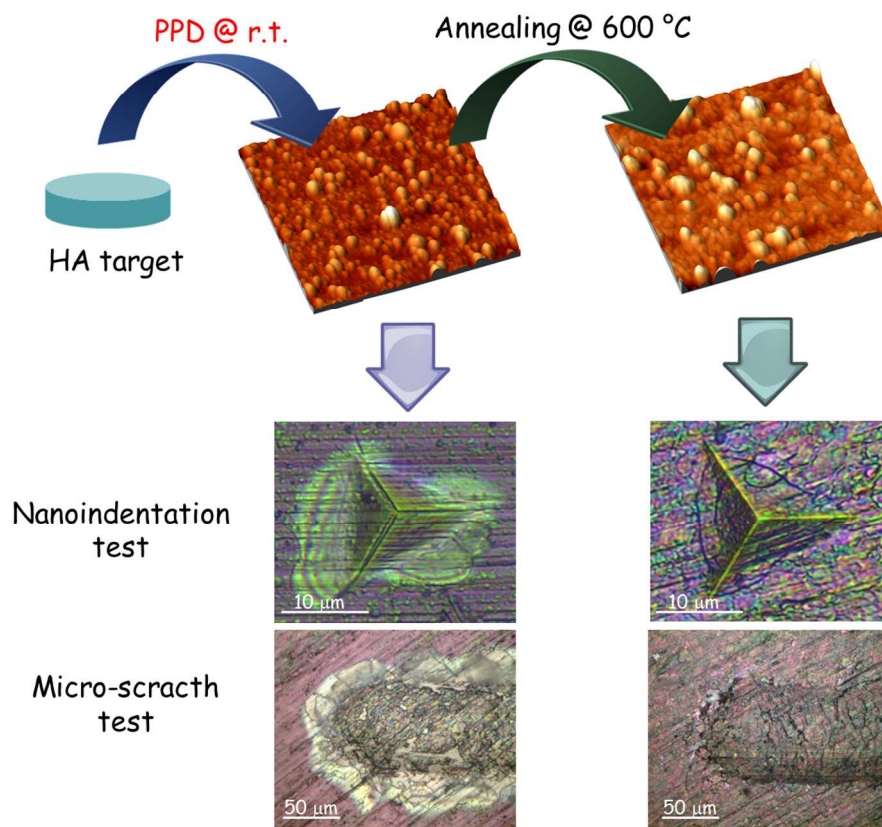


This is an *Accepted Manuscript*, which has been through the Royal Society of Chemistry peer review process and has been accepted for publication.

*Accepted Manuscripts* are published online shortly after acceptance, before technical editing, formatting and proof reading. Using this free service, authors can make their results available to the community, in citable form, before we publish the edited article. This *Accepted Manuscript* will be replaced by the edited, formatted and paginated article as soon as this is available.

You can find more information about *Accepted Manuscripts* in the [Information for Authors](#).

Please note that technical editing may introduce minor changes to the text and/or graphics, which may alter content. The journal's standard [Terms & Conditions](#) and the [Ethical guidelines](#) still apply. In no event shall the Royal Society of Chemistry be held responsible for any errors or omissions in this *Accepted Manuscript* or any consequences arising from the use of any information it contains.



Calcium phosphate thin films were deposited at room temperature by the Pulsed Plasma Deposition method. After annealing at 600 °C, film mechanical properties and adhesion to the titanium substrate strongly improved.

224x192mm (150 x 150 DPI)



## ARTICLE

Received 00<sup>th</sup> January  
20xx,

## Tough and adhesive nanostructured calcium phosphate thin films deposited by the Pulsed Plasma Deposition method

Marco Boi,<sup>a</sup> Michele Bianchi,<sup>a,\*</sup> Alessandro Gambardella,<sup>a</sup> Fabiola Liscio,<sup>b</sup> Saulius Kaciulis,<sup>c</sup> Andrea Visani,<sup>d</sup> Marianna Barbalinardo,<sup>e</sup> Francesco Valle,<sup>e</sup> Michele Iafisco,<sup>f</sup> Lisa Lungaro,<sup>g</sup> Silvia Milita,<sup>c</sup> Massimiliano Cavallini,<sup>e</sup> Maurilio Marcacci<sup>a</sup> and Alessandro Russo<sup>a</sup>

Accepted 00<sup>th</sup> January 20xx

DOI: 10.1039/x0xx00000x

[www.rsc.org/](http://www.rsc.org/)

Calcium phosphate (CaP) coatings are commonly employed to improve the bioactivity of bone and dental metal implants, due to the chemical-physical similarity with the mineral phase of bone, envisaged to enhance the integration with the surrounding bone tissue. However, growing concerns about the use of commercial thick CaP coatings, mainly related to their weak mechanical properties, poor interface strength and micro-structural inhomogeneity, are leading the investigation of new and alternative CaP deposition techniques. In this study the feasibility to deposit tough and well adherent CaP thin films by a novel Pulsed Plasma Deposition (PPD) method on Ti alloy was investigated. Microstructural, chemical and morphological properties of the coatings as well as the nano-mechanical properties and their adhesion to the Ti-alloy substrate were extensively characterized. *In vitro* biocompatibility was also preliminarily assessed evaluating the adhesion and proliferation of primary mouse osteoblasts. As-deposited CaP films were amorphous and exhibited dense and uniform surface composed of sub-micrometric aggregated globular particles. Noteworthy, mechanical properties of as-deposited films were comparable to the ones of commercial plasma-sprayed coatings despite the significant difference of thickness (a few hundred nanometers vs. tens of micrometers). After the thermal annealing of the as deposited films at 600°C for 1 h in air, a transformation from amorphous calcium phosphate to crystalline hydroxyapatite (HA) phase occurred. The mechanical properties as well as the adhesion to substrate of the annealed films strongly improved respect to those of the as deposited films, displaying interesting high hardness, elastic strain to failure and plastic deformation resistance values. Finally, biological *in vitro* tests indicated good biocompatibility of both as-deposited and annealed films, with this latter showing better cells adhesion and proliferation compared to the former.

### 1. Introduction

Metals such as stainless steel, cobalt-chrome alloys and titanium and its alloys are currently used to manufacture hip

and joint prostheses and dental implants (mainly artificial roots)<sup>1</sup>. Titanium alloys are often preferred, owing to their superior corrosion resistance and relative high strength, fatigue properties and bioinertness<sup>2</sup>. However, when a metallic implant is placed in the body, a non-physiological surface is introduced into the biological environment resulting in a mismatch of functional properties between living tissue and artificial materials<sup>3</sup>.

The common approach to overcome this problem and to improve the bioactivity of metal implants (i.e. increasing the bone-to-implant contact) is the introduction of an intermediate layer between the implant and the surrounding tissue that can resemble the physiological environment<sup>4</sup>. To this end, calcium phosphate (CaP) in the form of hydroxyapatite (HA) is the ideal candidate, due to the chemical similarity with bone mineral phase<sup>4,5</sup>.

<sup>a</sup> Laboratorio di NanoBiotecnologie (NaBi), Istituto Ortopedico Rizzoli, via di Barbiano 1/10, 40136 Bologna, Italy

<sup>b</sup> Istituto per la Microelettronica e i Microsistemi (IMM), Consiglio Nazionale delle Ricerche, via Gobetti 101, 40129 Bologna, Italy

<sup>c</sup> Istituto per lo Studio dei Materiali Nanostrutturati (ISMN), Consiglio Nazionale delle Ricerche, via Salaria km 29.300, PO Box 10, 00015 Monterotondo Staz. (RM), Italy

<sup>d</sup> Laboratorio di Biomeccanica ed Innovazione Tecnologica, Istituto Ortopedico Rizzoli, via di Barbiano 1/10, 40136 Bologna, Italy

<sup>e</sup> Istituto per lo Studio dei Materiali Nanostrutturati, Consiglio Nazionale delle Ricerche, via Gobetti 101, 40129 Bologna, Italy

<sup>f</sup> Istituto di Scienza e Tecnologia dei Materiali Ceramici, Consiglio Nazionale delle Ricerche, via Granarolo 64, 48018 Faenza (RA), Italy

<sup>g</sup> School of Engineering, Alrick Building, King's Buildings, West Mains Road, Edinburgh, Scotland.

\* Corresponding author;  
e-mail: m.bianchi@biomec.ior.it

Plasma spraying (PS) is by far the most widespread technology for the preparation of HA coatings for biomedical applications<sup>6</sup>. However, the high thickness of sprayed coating (from 50 to 200  $\mu\text{m}$ ) can introduce fatigue under tensile loading, while higher residual stresses and presence of voids can promote interfacial debonding and crack formation, respectively<sup>7</sup>. Further, the chemistry and micro-structure of HA sprayed coatings (usually consisting of both amorphous and different crystalline phase) are significantly different from bone mineral apatite, and can also lead to non-homogenous coating dissolution kinetics<sup>8</sup>. Finally, PS requires an additional roughening treatment of the metallic implant surface by sand or grit blasting to improve the adhesion of the coating to the implant by mechanically interlocking<sup>9</sup>; it follows that providing highly-adhered films without the need for such pre-treatments would be highly desirable. Moreover from a biological point of view, despite a plethora of works reporting the better behaviour both *in vitro* and *in vivo* of sprayed-coated devices compared to uncoated ones, long-term clinical data indicate that the actual clinical advantage of using PS coatings in implantology is still under debate<sup>10</sup>. Thus, the recent research trend is directed toward the deposition of high-performance CaP thin films (up to few microns thick), with improved adhesion, fracture toughness and lower residual stresses. Several technologies are currently available for the deposition of CaP thin films, such as pulsed laser deposition (PLD)<sup>11</sup>, radio frequency (RF)<sup>12</sup> or direct current (DC)<sup>13</sup> magnetron sputtering, electrospray deposition (ESD)<sup>14</sup> and ion beam-assisted deposition (IBAD)<sup>15</sup>.

Recently, the Pulsed Plasma Deposition (PPD) technique has been emerging as a valid technique for the stoichiometric deposition of well adherent and nanostructured thin films of a number of materials<sup>16, 17</sup>. The working principle of PPD is based on the ablation of a target material by a highly-energetic pulsed electron beam; consequently, the ablated material is deposited on a substrate hold at suitable distance. The pulsed ablation process allows obtaining a high control on the final film thickness and roughness<sup>18</sup>. PPD is conceptually similar to the more widespread PLD but when compared to the latter it presents several advantages, as a direct consequence of the different nature of the ablating source: higher pulse energy, frequency and energy efficiency (>30%); capability to ablate wide band-gap or highly reflective materials ( $E_g > 6 \text{ eV}$ ); easier scalability of the process for the deposition of large area by relatively low-cost multiple systems. Since its introduction at the end of the first decades of 2000s, PPD has been exclusively used for the fabrication of thin films in the field of photovoltaic and

organic electronics<sup>19, 20</sup>. Very recently, the first medical application of PPD was reported, with the specific aim of decreasing the wear of the mating components of an implant joint replacement by coating their surfaces with hard zirconia films<sup>21-23</sup>.

Due to requirement of alternative solutions to obtain enhanced performing bioactive CaP coatings, and in order to investigate the possibility to deposit nanostructured thin films with improved mechanical properties, in this study the deposition and characterization of HA films via the PPD method has been investigated. Specifically, crystalline structure, chemical composition, surface morphology, nano-mechanical properties and adhesion of as-deposited and thermally annealed films have been addressed and the results discussed in the light of the performances of conventional HA coatings.

## 2. Experimental

### 2.1 Materials

CaP thin films were deposited by ablating a HA target sintered at 1200 °C in air (Ca/P = 1.67, Institute of Science and Technology for Ceramics – National Research Council, Faenza, Italy). Titanium alloy disks (grade 2,  $\varnothing \sim 15 \text{ mm}$ , thickness  $\sim 5 \text{ mm}$ ,  $R_a \sim 1 \text{ micron}$ , water contact angle  $\sim 73^\circ$ ) and silicon wafers (p-type doped monocrystalline (100) native silicon, p-type, size  $\sim 20 \times 20 \text{ mm}$ , thickness  $\sim 3 \text{ mm}$ , Fondazione Bruno Kessler, Trento, Italy) were used as substrates, after being ultrasonically cleaned in acetone, isopropanol and dried under nitrogen flux.

### 2.2 Film deposition and thermal annealing

The setup of the Pulsed Plasma Deposition (PPD) system (Gen III Advanced Electron Gun, Organic Spintronics, Bologna, Italy) is schematically depicted in **Fig. 1** and has been described in detail elsewhere<sup>16, 21</sup>. The vacuum chamber was initially voided down to a pressure of  $1 \times 10^{-6}$  mbar by using a turbo-molecular pump (EXT255H, Edwards, Crawley, England). Then the pressure was raised to the working value by introducing in the chamber the working gas (oxygen, purity level: 99.999 %). After a preliminary deposition set aimed to optimize deposition parameters, the working gas pressure, the beam acceleration voltage and the shot frequency were set at  $3 \times 10^{-4}$  mbar, 16.0 kV and 5 Hz, respectively. Target-substrate distance was set at 60 mm, in order to allow a wide and uniform coverage of the substrate. Deposition was performed without heating the substrate. A very low thickness such as 300 nm was selected in order to maximize the comparison between the properties of the HA

films deposited by PPD and thicker films deposited by conventional methods. After deposition, films were annealed at 600 °C for 1 h in air, using a ramp of 20°C/min both for the heating and the cooling steps. As-deposited films are hereinafter referred as CaP<sub>rt</sub>, whereas annealed films are referred as CaP<sub>600</sub>.

### 2.3 Structural and morphological characterization

The structural characterization of CaP<sub>rt</sub> and CaP<sub>600</sub> films was performed by X-Ray Diffraction (XRD) in out-of-plane and grazing incidence geometry, using a SmartLab Rigaku diffractometer equipped with a rotating anode (Cu K $\alpha$ ,  $\lambda$  = 1.54180 Å). The incidence angle was 0.8° in order to penetrate the whole film and to reduce the scattering coming from the substrate.

Small amount of CaP films were manually removed from titanium disks and analyzed by Fourier transform infrared (FTIR) spectroscopy. Spectra were recorded on a Thermo Nicolet 380 (Thermo Fisher Scientific Inc., Waltham, USA) spectrometer. The powder sample (about 1 mg) was mixed with about 200 mg of anhydrous KBr and pressed into 7 mm diameter discs. Spectra were registered with a resolution of 4 cm<sup>-1</sup> by accumulation of 64 scans covering the 4000 to 400 cm<sup>-1</sup> range.

Film chemical composition was evaluated by X-ray photoelectron spectroscopy (XPS) using an ESCALAB 250Xi spectrometer (Thermo Fisher Scientific, UK), equipped with monochromatic Al K $\alpha$  excitation source and a 6-channeltron spectroscopic detection system. Photoelectron spectra were collected at 20 eV constant pass energy of the analyzer and a base pressure in the analysis chamber of about 5 x 10<sup>-8</sup> Pa. XPS measurements were carried out at 90° take-off angle, by using a large spot of X-ray source (diameter of 0.9 mm) and electromagnetic lens mode resulting in 0.5 mm diameter of analyzed sample area. The sample charging was suppressed by using in-lens electron flood gun at low energy of 1 eV. The accuracy of experimental binding energy (BE) scale was  $\pm$  0.1 eV. Distribution of the chemical composition in depth was investigated by combining the XPS analysis and cyclic Ar<sup>+</sup> sputtering at energy of 2.0 keV. Spectroscopic data were processed by the Avantage v.5 software. Shirley background and mixed Lorentzian/Gaussian peak shape (30%) were used for the peak fitting.

Microstructural and morphological characterization of the coatings was carried out by field emission gun scanning electron microscopy (FEG-SEM) using a Sigma NTS GmbH (Carl Zeiss, Germany). Before the analyses the specimens were covered with a coating of Au using a Sputter Coater E5100 (Polaron Equipment, Hertfordshire, U.K.).

Film thickness and surface roughness were evaluated by Atomic Force Microscopy (AFM), using an NT-MDT Stand-alone AFM operating in semi-contact mode at ambient conditions. As force sensors for imaging, different NT-MDT Si-cantilevers with curvature radius of 10 nm and resonance frequencies of (190 – 330) kHz were used. All images were unfiltered but levelled by a 2<sup>nd</sup> order line, and acquired with a resolution of 512 x 512 pixels. The Average Roughness (R<sub>a</sub>) value was provided as estimate of surface roughness.

Film wettability was addressed by contact angle measurements carried out using a contact angle meter Digidrop from GBX (Bourg de Peage, France) The measurements were taken at 25°C and the Milli-Q water drops were 1  $\mu$ l.

### 2.4 Nano-mechanical characterization

The mechanical properties of as-deposited and annealed films were investigated by nanoindentation tests using a Nanoindenter Tester NHT<sup>2</sup> (CSM, Peseux, Switzerland) equipped with a Berkovich diamond tip, after a preliminary calibration performed on a standard fused silica (plain strain modulus  $\sim$  (75.1  $\pm$  0.4) GPa; estimated silica Poisson's ratio of 0.16). For nanoindentation tests, silicon was preferred, due to the very flat surface compared to the surface of titanium disks allowing a smaller data deviation. The indents were performed using a standard trapezoidal linear-loading profile up a maximum load (P<sub>max</sub>) of 0.75 mN followed by a pause of 2 s with a loading/unloading time of 10 s. Indentation hardness (H<sub>IT</sub>) and elastic modulus (E<sub>IT</sub>) were extracted from the recorded load-displacement curve using the well-established Oliver and Pharr method<sup>24</sup>. Subsequently, the elastic strain to failure (H/E) and the resistance to plastic deformation (H<sup>3</sup>/E<sup>2</sup>) were calculated.

In order to evaluate film fracture toughness on titanium substrate, specific nanoindentation tests using increasing P<sub>max</sub> (1, 5, 25, 50, 100 and 500 mN) have been performed. In particular, the maximum penetration depth achieved by the indenter tip within the film has been investigated. Each loading and loading rate was set to 10 s with a pause of 2 s at P<sub>max</sub>. An optical microscope (equipped with objectives from 1x to 100x) mounted on the nanoindentation platform was used to image the footprint left by the indenter on the sample surface.

### 2.5 Adhesion tests

To evaluate film adhesion to the titanium substrate, scratch tests were performed using a Micro-scratch Tester MST (CSM, Peseux, Switzerland), equipped with a Rockwell C stylus conical with spherical apex indenter tip (radius sphere

100  $\mu\text{m}$  and angle  $120^\circ$ ). The tip was subjected to a progressive normal load from 0.01 to 3.00 N were move across a surface with scan speed of 10 mm/min and a loading rate of 10 mN/min according to the ASTM C 1624-05<sup>25</sup>. A minimum of three scratches were made on each investigated film. The employed test mode entailed a pre-scan of the surface with a small load (10 mN) to store the surface profile, which was eventually subtracted from the loaded scratch scan. Then the indenter performed the real scan linearly increasing the load according to the previously reported loads. An optical microscope (equipped with objectives form 1x to 100x) mounted on the micro-scratch platform was used to image the worn track left by the micro-scratch tip on the sample surface and investigate the delamination modes of the film the different loads (0.5, 1.5 and 3N).

## 2.6 Isolation and Culture of Primary Bone Cells

Primary osteoblasts were isolated from the calvarial bones of 1 week-old mice by sequential collagenase digestion as described elsewhere<sup>26</sup>. Briefly the calvarial bones were digested in collagenase type 1 at  $37^\circ\text{C}$  with three consecutives washes. The cell suspension were pooled and centrifuged at 300 rpm for 3 minutes. The supernatant was discarded and cell pellets were suspended in standard  $\alpha\text{MEM}$  supplemented with 10% FCS with Penicillin-Streptomycin (10,000 U/mL). The cell suspension was cultured under standard condition in a 25  $\text{cm}^2$  tissue culture flask at a density of 1 calvaria per flask. The medium was changed 24 hours after seeding to remove non-adherent cells, and then every 48 hours until they reached the confluence. Cells were incubated in  $\alpha\text{MEM}$ , supplemented with 10% fetal bovine serum, 2mM L-glutamine, 100 U  $\text{ml}^{-1}$  penicillin and 100  $\mu\text{g ml}^{-1}$  streptomycin, in a humidified atmosphere (95% air, 5%  $\text{CO}_2$ ,  $37^\circ\text{C}$ ).

## 2.7 Cell seeding

Primary osteoblast cells were cultured in  $\alpha\text{MEM}$ , supplemented with 10% fetal bovine serum, 2mM L-glutamine, 100 U  $\text{ml}^{-1}$  penicillin and 100  $\mu\text{g ml}^{-1}$  streptomycin. After 4 days in culture, cells were trypsinized and plates over the CaP<sub>rt</sub> and CaP<sub>600</sub> films (in addition to control substrates) at a density of 5000 cell  $\text{cm}^{-2}$  using 24-well plates. Cultures were grown at  $37^\circ\text{C}$  in an atmosphere of

5%  $\text{CO}_2$ , 95% air for 3h, 24h, 48h and 72h and the medium was changed every 24h.

## 2.8 Immunofluorescence assay

Prior to the immunofluorescence assay, each samples was carefully placed in a new 24 multi-well plate to eliminate any contribution of remnant cells from the cell suspension. Cells were fixed with 4% paraformaldehyde in DPBS 1x, washed with DPBS 1x. They were then permeabilized with 0.1% Triton-X 100. The samples incubated in 1% bovine serum albumin in DPBS 1x to block non-specific binding sites. Double staining was then performed on each sample. Cells were first stained by Vinculin monoclonal antibody (FAK100, Merck Millipore), followed by rinses with DPBS 1x. The cells were labelled with FITC-anti-mouse IgG antibody (AP124F, Millipore) in combination with TRITC-conjugated phalloidin (FAK100, Merck Millipore) for 1 h, followed by rinses with DPBS 1x. Double staining was critical to map local orientation of actin filaments within cells and a monoclonal antibody to Vinculin was very specific for staining the focal contacts in cells. Nuclear counterstaining was performed by incubation with DAPI (FAK100, Merck Millipore) for 3 min, followed by rinses with DPBS 1x. Samples were examined using a Nikon Eclipse 80i microscope equipped for fluorescence analysis.

## 2.9 Statistical analysis

Data from in vitro tests were presented as means  $\pm$  standard deviations (SD). Comparison between groups was carried out with the Wilcoxon rank sum non-parametric test ( $p < 0.05$ ) MATLAB software (version: 8.2.0.701, Mathworks, Natik, MA).

## 3. Results

### 3.1 Microstructural, chemical and morphological characterization

XRD analyses revealed that the CaP<sub>rt</sub> films were mainly amorphous (Fig. 2a-i), as evinced by the broad peak spanning from  $25^\circ$  to  $35^\circ$ . The presence of CaO crystallites was evidenced by the Bragg peaks observed at  $32.5^\circ$  and  $37.4^\circ$  (ICSD: 060199). Also a small amount of  $\text{Ca}(\text{OH})_2$  crystallites were detected (peak at  $28.45^\circ$ , ICSD: 202233). After a thermal annealing in air at  $600^\circ\text{C}$  for 1h, a polycrystalline HA film was obtained. Indeed, the XRD pattern (Fig. 2a-ii) showed all the main peaks characteristic of the HA crystal

phase (ICSD: 081442). However, the main peak coming from CaO crystallites were still detected after annealing.

FTIR spectra of the deposited materials showed the typical bands of CaP compounds [(i.e.  $\text{PO}_4^{3-}$  vibration bands at 560–603 ( $\nu_4$ ), 963 ( $\nu_1$ ), and 1000–1104  $\text{cm}^{-1}$  ( $\nu_3$ )]<sup>27</sup> (Fig. 2b). In agreement with the XRD analyses, the FTIR spectra of CaP<sub>rt</sub> displayed the characteristic broad bands of amorphous CaP phase<sup>28</sup> (Fig. 2b-i), that after the annealing, became more narrow and defined revealing that the amorphous phase turned into a crystalline state (Fig. 2b-ii). The appearance of the band at 630  $\text{cm}^{-1}$ , assigned to vibration of structural OH<sup>-</sup> groups, in the CaP<sub>600</sub> sample also confirmed the transformation from an amorphous to a crystalline phase.

XPS data on the surface composition (Table 1) revealed the signals of Ca 2p, P 2p and O 1s that are the characteristic photoemission peaks of the CaP phases. Their BE values correspond to those reported in previous works<sup>29, 30</sup> within the margins of experimental errors. The different Ca/P ratio between CaP<sub>rt</sub> and CaP<sub>600</sub> confirmed the occurrence of a phase transition process. However, the spectra of Ca 2p and O 1s were quite broad, i.e. indicated the possible presence of more than one chemical species.

More detailed analysis of chemical composition was carried out by using XPS depth profiling and applying the peak fitting procedure for broad Ca 2p and O 1s spectra. The deconvolution of both peaks after 300 s of ion sputtering (depth of about 50 nm) is presented in Fig. 3a and 3b. The lower components Ca1 and O1 can be attributed to the presence of CaO, which is also evidenced by the XRD analysis. The dominant species Ca2 and O2 correspond to HA<sup>29, 30</sup>. Obtained elemental depth profile with separated different species of Ca and O is reported in Fig. 3c. As it can be observed in this profile, the surface contamination (adventitious carbon) was already removed after the first cycle of ion sputtering (depth of about 5 nm), afterwards the chemical composition of the film became constant till the interface with substrate (not shown in this figure) at the depth of about 280 – 300 nm. After removal of contaminant over layer, the total ratio Ca/P was about 2.1, but the ratio of the species attributed to HA Ca2/P was almost stoichiometric (1.68 – 1.74).

FEG-SEM analyses (Fig. 4) revealed that the surface of the CaP<sub>rt</sub> was dense and uniform composed of sub-micrometric aggregated globular particles ranged from 50 to 300 nm. The surface morphology of the coatings was independent on the annealing temperature; in fact no significant differences were found comparing micrographs of CaP<sub>rt</sub> and CaP<sub>600</sub>.

AFM analysis (Fig. 5) indicated that CaP<sub>rt</sub> showed a highly-homogeneous granular texture of the surface (Fig. 5a), with densely packed ~ 50 - 100 nm sized-grains, occasionally aggregating to form larger particulate (size ~ 300 nm), in agreement with the FEG-SEM observations. The annealing process did not produce significant morphological changes at the macro-scale (Fig. 5b), as indicated by the average roughness calculated on a 50 x 50  $\mu\text{m}^2$  scan area, that was similar between CaP<sub>rt</sub> and CaP<sub>600</sub> (Fig. 5c). At the micro-scale, the surface roughness of CaP<sub>600</sub> was slightly lower than the roughness of CaP<sub>rt</sub>, as a consequence of a starting thermally induced grain coalescence process.

Contact angle measurements of films deposited on titanium disks (whose bare surface was hydrophobic with a contact angle of about 73°) showed that the deposition of the CaP layer lowered the contact angle value to (50 ± 1)°, as expected. Interestingly, the thermal treatment led to a further significant increase in wettability, since the contact angle value was 23 ± 2°, which is a typical value for a hydrophilic material. Being the macro-scale roughness similar between CaP<sub>rt</sub> and CaP<sub>600</sub>, the change of the contact angle value can be ascribed to the decrease of micro-scale roughness caused by the thermal treatment.

### 3.2 Nanoindentation tests

Film hardness increased after the annealing treatment, whereas a slight decrease of the elastic modulus was registered (Table 2). As a consequence, the elastic strain to failure (H/E) and the resistance to plastic deformation ( $H^3/E^2$ ) increased from 0.035 to 0.060 and from 0.005 to 0.018, respectively, indicating a general improvement of mechanical properties after the thermal treatment.

In Fig. 6a, the indentation load-depth curves for CaP<sub>rt</sub> and HA<sub>600</sub> applying a 5 mN load are depicted: due to improved mechanical properties after annealing, the penetration depth of the indenter tip for CaP<sub>600</sub> was half of the penetration depth for CaP<sub>rt</sub>.

Indentation depth values vs. applied load are reported in Fig. 6b: at the same load, the indenter tip penetrated to a lower extent for the annealed film compared to the as-deposited film. In particular, the gap between the two samples was maximized when using a load of 25 mN and became smaller at high loads as a consequence of the more prominent effect of the mechanical properties of the substrate on the measured value. Data for CaP<sub>rt</sub> were well-fitted by a power law ( $y = 166,4x^{0,4342}$ ;  $R^2 = 0,9996$ ) whereas data for CaP<sub>600</sub> could be better fitted by a polynomial function ( $y = -0,0246x^2 + 12,906x + 113,12$ ;  $R^2 = 0,9987$ ), indicating a close-to linear

dependence of the indentation depth upon applied load with respect to HA\_rt.

Finally, fracture toughness tests were carried out in order to assess the ability to as-deposited and annealed films to withstand high loads (Fig. 6c and 6d). When applying a high load as 500 mN, whereas on the as-deposited film pile-up and film detachment phenomena occurred (white and arrow in 4c, respectively), only internal cracks were visible in the annealed samples, with no detachment at all of the film. This fact suggested, besides high fracture toughness, a very good adhesion to the substrate, which is a key property for a bioactive HA thin film.

### 3.3 Micro-scratch tests

Film adhesion was better addressed by specific micro-scratch tests, in which a diamond tip performs a scratch on the surface of the film applying an increasing load up to the detachment of the film. CaP\_rt films showed lower scratch resistance than CaP\_600 coatings (Fig. 7). For instance, at a load of 0.5 N, whereas on the annealed sample (vi) only minor surface modification were visible, clear signs of initial film detachment appeared on the as-deposited films (iii). Similarly, at 1.5 N, whereas the surface of CaP\_rt was already strongly compromised (ii), only small ductile tensile cracking<sup>31</sup> were visible on the surface of HA\_600 (v, white arrows). At the max load (3 N), wedging/spallation phenomena were well recognizable in the as-deposited film (i, black arrows) and the film was completely detached inside the worn track; on the contrary no film spallation occurred in the annealed samples, and the film was only cracked by still adhered to the titanium substrate (iv).

### 3.4 Cells viability and adhesion

Osteoblasts adhesion and proliferation up to 72h was evaluated to preliminary assess the biocompatibility of CaP and CaP\_600 films. No significant differences were detected in cellular proliferation among all the groups even after 3 days of culture, even if the cells adhesion and proliferation was generally higher on CaP\_600 compared to CaP\_rt (Fig. 8a). This trend was confirmed by immunostaining images (Fig. 8b-d), which showed more cells adhesion on CaP\_600 than on CaP\_rt. Cytoskeleton staining showed well developed actin filaments and the focal adhesion points were already high at 3h on CaP\_600 (Fig. 8b), whereas cells were still not fully spreaded on CaP\_rt at 24h (Fig. 8c). Images at 72h indicated the formation of connections

between adjacent cells in both the samples, more developed for cells seeded on CaP\_600 (Fig. 8d), less for CaP\_rt (data not shown).

## 4. Discussion

In this work, CaP thin films were deposited by the Pulsed Plasma Deposition method and the structural, chemical, morphological and mechanical properties of as-deposited and annealed films were analyzed.

CaP films deposited at room temperature exhibited a nearly amorphous structure whereas, after annealing at 600°C for 1 hour in air, a crystalline HA structure was produced. Interestingly, the accessories phases (i.e. CaO and Ca(OH)<sub>2</sub>) strongly reduced their relative intensities in the annealed films. PS process can produce either amorphous or crystalline HA coatings depending on the structure of the starting materials and the deposition parameters<sup>6</sup>. When treated at 600° C in air PS coatings show the significant presence of CaO within the coating, because CaO cannot be easily converted into HA without the massive presence of water molecules in the heating atmosphere<sup>32</sup>. Instead, physical vapor deposition methods such as PLD and magnetron sputtering usually produce amorphous films when not heating the substrate at several hundreds of degrees<sup>33</sup>. This fact can be ascribed to the complete vaporization of the target material: expelled ions and atoms have to efficiently rearrange according to a crystalline structure in the growing film by exploiting the kinetic energy provided by the vaporization method. Unfortunately, when performing the deposition at room temperature, the kinetic energy of the incoming ions and atoms is not usually sufficient to lead the atoms rearrangement according to a well-defined crystalline structure, and amorphous films are obtained. Thus, it is common procedure to perform thermal or laser annealing post deposition treatments to enhance film crystallinity and avoid rapidly-dissolving amorphous HA films which can lead to detrimental implant mobilization<sup>34</sup>. PPD has been already demonstrated to be able to provide highly-crystalline films of zirconium oxide even at room temperature<sup>21</sup>, thanks to the higher kinetics involved in the deposition process<sup>16</sup>. However, the more complex crystalline structure and chemical composition of HA compared to zirconia as well as the presence of easy-to-form competitor phases, did not allow to deposit crystalline HA films at room temperature and a thermal annealing to improve crystallinity is required.

The Ca/P ratio of deposited films (1.45) increased after annealing (1.96), due to the presence of additional phases,

as suggested by the broad peaks of Ca and P in the XPS peaks. The chemical composition of HA films deposited by PS, magnetron and PLD techniques can exhibit very different Ca/P ratio, even within the same method, ranging from 1.1 to  $\sim 3$ <sup>33</sup>. This significant variation is a consequence of the effect of several factors such as deposition temperature, pressure, and working gas that can affect and accelerate the formation of accessories phase such as CaO and Ca<sub>3</sub>(PO<sub>4</sub>)<sub>2</sub>, leading to a Ca/P ratio decrease, or the preferential deposition of calcium rather than phosphorous, leading to a Ca/P increase. It has been also demonstrated that the Ca/P ratio generally increases with annealing temperature<sup>34</sup>. Thus, it can be inferred that the Ca/P value found in this study for CaP<sub>rt</sub> is due to the significant presence, demonstrated by XRD analysis, of CaO and Ca(OH)<sub>2</sub> in the as-deposited films and not to loss of volatile species contacting phosphorous such as P<sub>2</sub>O<sub>5</sub> during deposition<sup>35</sup>. Besides, the rise of the Ca/P ratio after annealing can be attributed to a loss of phosphate groups at high temperatures.

Micro- and nano-topography play a key role on the ability of the coating to promote new bone apposition<sup>36, 5</sup>. In particular, the nanoscale morphology has been demonstrated to have a positive impact on bone tissue regeneration<sup>37</sup>. The morphological and microstructural analysis carried out by FEG-SEM and AFM revealed that as-deposited and annealed films prepared in this work showed nanostructured morphology, with small and densely packed CaP grains, similar to those observed in the sputtered CaP films<sup>33</sup> and in contrast with micro-rough porous coatings made by PLD and PS<sup>34</sup>. In addition to improved biological activity, it was demonstrated that nanostructured surfaces confer improved fracture toughness and resistance to crack formation to the coatings<sup>39</sup>.

In order to establish the ability of thin films of HA to withstand mechanical loads, nanoindentation tests with maximum applied load were performed. Nanoindentation tests are useful to characterize the mechanical properties of materials at the micron and sub-micron scale, being an ideal candidate to test to evaluate the nano-mechanical properties of thin films. Once the hardness (H) and elastic modulus (E) have been calculated, one can obtain the elastic strain to failure (H/E), and the resistance to plastic deformation (H<sup>3</sup>/E<sup>2</sup>), two parameters that have been increasingly used to describe the overall mechanical behavior of films and coatings, beyond the only hardness of modulus value<sup>40, 41</sup>. In the present study, due to the fact the H was higher whereas E was lower after the thermal annealing process, H/E and H<sup>3</sup>/E<sup>2</sup> ratios for CaP<sub>600</sub> were more than two and three times higher than for CaP<sub>rt</sub>. This clearly indicates an overall

improvement of the mechanical properties of the HA films when treated for 1h at 600 °C in air. In literature, a wide range of H values is reported for PS coatings, from 1.5 GPa (amorphous HA)<sup>42</sup> to 9.8 GPa (laser processed HA)<sup>43</sup>. However, the vast majority of the papers reports values of about 3 - 5 GPa for H<sup>44, 45</sup>. As above-mentioned, PLD has a similar setup when compared to PPD that makes the comparison of the mechanical properties of deposited films more reliable. HA films deposited by PLD show hardness values ranging from 1.3-1.9 GPa when heating the substrate at 400°C<sup>46</sup>, up to 2-3 GPa when heating the substrate at 650°C<sup>12</sup>. Similar conclusions can be made for what the H/E and H<sup>3</sup>/E<sup>2</sup> values are concerned. Thus, mechanical properties HA films deposited at room temperature in our study, were already in line with conventional values for PS coatings, despite a reduction of about three orders of magnitude in thickness, and generally higher than reported values for PLD. It is also worthwhile to remind that, after annealing, the mechanical properties of the HA films even significantly improved.

A good adhesion of the HA film or coating to the Ti substrate is a fundamental prerequisite for long-term standing coated-implants. Micro-scratch tests are frequently used to evaluate the adhesion of a film to the substrate. By imposing a steady or increasing load, the crack formation onset and the film buckling and delamination can be observed. Here, annealed HA films clearly exhibited a higher scratch resistance when compared to as-deposited films, as evidenced by the absence of significant delamination even at the maximum load (3N), indicating a strongly bonded HA layer on the Ti substrate. The comparison with literature data concerning scratch tests is hindered by the scarcity of data available and to the very different experimental parameters used (max load, loading rate, scratch length, etc.). In general, HA thin films made by physical vapor deposition techniques such as magnetron and PLD exhibit higher adhesion to the substrate compared to PS coatings, due to the higher energy of the nano-particles impinging the surface of the substrate<sup>32</sup>. For instance, Pichugin and co. investigated the scratch resistance of HA films deposited by radio frequency magnetron sputtering at 500°C on Ti<sup>47</sup>, finding that the adhesion strength the coatings to the substrate depended on coating thickness and decreased for larger thickness than 1.6 μm.; no film exfoliation was observed till the max load (2N). Dinda and co. instead reported the scratch resistance of HA films (1 micron thick) deposited by PLD on Ti<sup>36</sup>. No significant differences were detected about strength resistance of as-deposited amorphous and annealed crystalline films, with no delamination but only minor cracks up to the max load of 2N.

The authors ascribed the good adhesion of the film to the low temperature process, that restricted the formation of Ti-oxide compounds at the interface between the coating and substrate that are envisaged to compromise the adhesion of the HA layer<sup>48</sup>. It is rationale to believe that this was the same reason that lied behind the good adhesion strength provided by the HA films described in this work.

Finally, *in vitro* cells test indicated similar biocompatibility of both as-deposited and annealed films. However, cell morphology as well as development of actin filaments was more pronounced in the cells seeded on the annealed films, suggesting a positive effect of the thermal annealing process over the biological properties of deposited calcium phosphate films.

### Conclusions

Highly-homogeneous and nanostructured CaP thin films were deposited by the PPD method. Interestingly, HA films prepared after the annealing at 600°C of the as-deposited coatings at room temperature, showed comparable mechanical properties with respect to commercial PS coatings, despite the very small thickness, and promisingly high values when compared to similar techniques such as PLD. The reported results suggest further investigations about the use of CaP films realized by PPD as a reliable alternative to conventional bioactive coatings in the orthopedic and dental fields.

### Acknowledgements

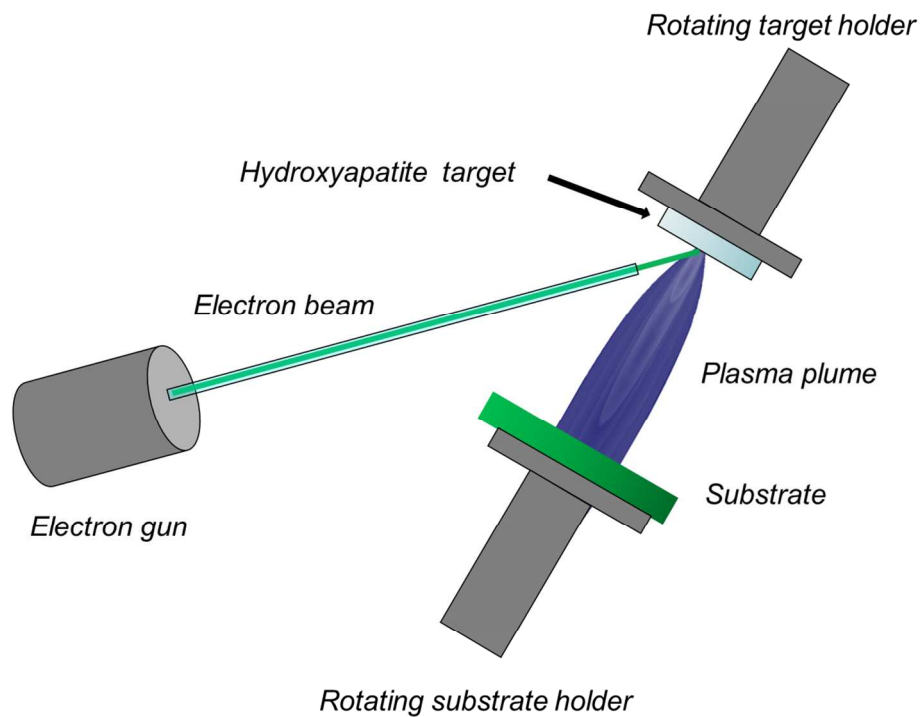
This study was supported by the project “Nanostructured Coatings Enhancing Material Performances in Joint Arthroplasty” (project code: 2012-1838), co-funded by the Italian Ministry of Health. This work was also partially supported by National flagship: NANOMAX N-CHEM. The authors would like to particularly thank Mr. Carmelo Carcasio for the technical upgrades of the deposition system.

### References

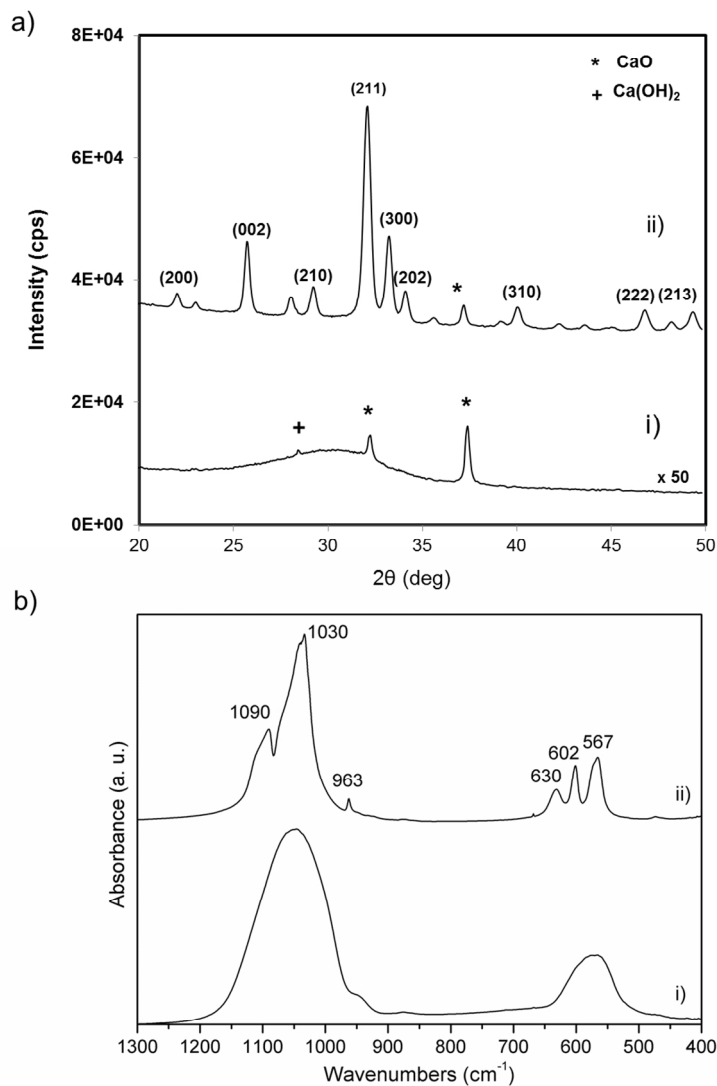
- 1 M. G. Zywiell, S. A. Sayeed, A. J. Johnson, T. P. Schmalzried and M. A. Mont, *Clin. Orthop. Rel. Res.*, 2011, **469**, 1536;
- 2 M. Niinomi, *J. Mech. Behav. Biomed. Mater.*, 2008, **1**, 30;
- 3 L. T. de Jonge, S. C. G. Leeuwenburgh, J. G. C. Wolke and J. A. Jansen, *Proceedings of the Institution of Mechanical Engineers, Part H: Journal of Engineering in Medicine*, 1998, **212**, 137;

- 4 H. Daugaard, B. Elmengaard, J. E. Bechtold and K. Soballe, *J. Biomed. Mater. Res. A*, 2008, **87**, 434;
- 5 M. Bianchi, E. R. Urquia Edreira, J. G. C. Wolke, Z. T. Birganic, P. Habibovic, J. A. Jansen, A. Tampieri, M. Marcacci, S.C.G. Leeuwenburgh and J. J. J. P. van den Beucken, *Acta Biomater.*, 2014, **10**, 661;
- 6 L. Sun, C. C. Berndt, K. A. Gross and A. Kucuk, *J. Biomed. Mater. Res. A* 2001, **58**, 570.
- 7 Y. C. Tsui, C. Doyle and T. W. Clyne, *Biomater.*, 1999, **19**, 2031;
- 8 W. Tong, J. Chen, X. Li, Y. Cao, Z. Yang, J. Feng and X. Zhang, *Biomater.*, 1996, **17**, 1507;
- 9 J. S. Hermann, J. D. Schoolfield, R. K. Schenk, D. Buser and D. L. Cochran, *J. Periodont.*, 2001, **72**, 1372;
- 10 S. Lazarinis, J. Kärrholm and N. P. Hailer, *Acta Orthop.*, 2011, **82**, 399;
- 11 D. V. Shtansky, N. A. Gloushankova, A. N. Sheveiko, Ph. V. Kiryukhantsev-Korneev, I. A. Bashkova, B. N. Mavrin, S. G. Ignatov, S. Yu. Filippovich and C. Rojas, *Surf. Coat. Tech.*, 2010, **205**, 728;
- 12 H. Kim, R. P. Camata, S. Chowdhury and Y. K. Vohra, *Acta Biomaterialia*, 2010, **6**, 3234;
- 13 M. A. Surmeneva, A. Kovtun, A. Peetsch, S. N. Goroja, A. A. Sharonova, V. F. Pichugin, I. Y. Grubova, A. A. Ivanova, A. D. Teresov, N. N. Koval, V. Buck, A. Wittmar, M. Ulbricht, O. Prymak, M. Epple and R. A. Surmenev, *RSC Adv.*, 2013, **3**, 11240;
- 14 M. Iafisco, R. Bosco, S. C. G. Leeuwenburgh, J. J. J. P. van den Beucken, J. A. Jansen, M. Prat and N. Roveri, *Adv. Eng. Mater.*, 2012, **14**, B13.
- 15 T. R. Rautray, R. Narayanan, T. Y. Kwon and K. H. Kim. *J. Biomed. Mater. Res. B*, 2010, **93**, 581;
- 16 D. Yarmolich, P. Nozar, S. Gleizer, Y. E. Krasik, G. Mittica, C. Ancora, A. Brillante, I. Bilotti and C. Taliani, *Jap. J. Appl. Phys.*, 2011, **50**, 08JD03;
- 17 E. Arisi, I. Bergenti, M. Cavallini, M. Murgia, A. Riminucci, G. Ruani, V. Dediu, *J. Magn. Magn. Mater.* 2007, **316**, 410;
- 18 Cavallini, M. *et al.* Selective electrochemical decomposition of outgrowths and nanopatterning in La<sub>0.7</sub>Sr<sub>0.3</sub>MnO<sub>3</sub> perovskite thin films. *Scientific Reports* **4**, doi:10.1038/srep07397 (2014).
- 19 Y. W. Huang, Q. Zhang, J. H. Xi and Z. G. Ji, *Appl. Surf. Sci.*, 2012, **258**, 7435.
- 20 M. Yang, H. F. Pu, Q. F. Zhou and Q. Zhang, *Thin Solid Films* 2012, **520**, 5884.
- 21 M. Bianchi, A. Russo, N. Lopomo, M. Boi, M. C. Maltarello, S. Sprio, M. Baracchi and M. Marcacci, *J. Mater. Chem. B*, 2013, **1**, 310;
- 22 M. Bianchi, M. Boi, N. Lopomo, M. C. Maltarello, F. Liscio, S. Milita, A. Visani, A. Russo and M. Marcacci, *J. Mech. Med. Biol.*, 2015, **15**, 1550070;
- 23 M. Bianchi, N. Lopomo, M. Boi, A. Gambardella, G. Marchiori, M. Berni, P. Pavan, M. Marcacci and A. Russo, *J. Mech. Med. Biol.*, 2015, **15**, 1540002.

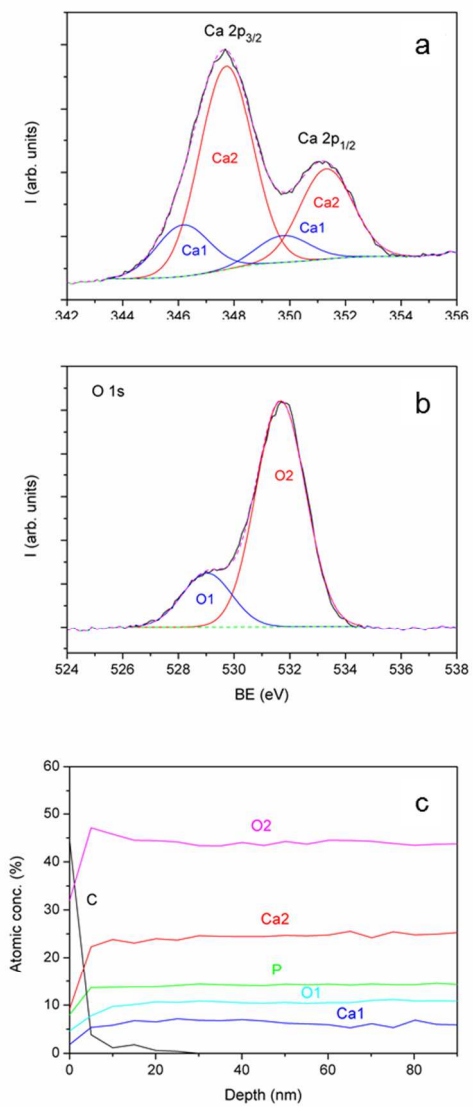
- 24 W. C. Oliver and G. M. Parr, *J. Mater. Res.*, 2004, **19**, 3;
- 25 P. Kutilek and . Miksovsky, *Acta Bioeng. Biomech.*, 2011, **13**, 87;
- 26 A. Bakker and J. Klein-Nulend, in *Bone Research Protocols*, ed. M. H. Helfrich and S.H. Ralston, Humana Press, Totowa, New Jersey, 1988, pp. 19–28;
- 27 M. Iafisco, J. Gómez Morales, M. A. Hernández-Hernández, J. M. García-Ruiz and N. Roveri, *Adv. Eng. Mater.*, 2010, **12**, B218;
- 28 C. Combes and C. Rey, *Acta Biomater.*, 2010, **6**, 3362;
- 29 S. Kaciulis, G. Mattogno, A. Napoli, E. Bemporad, F. Ferrari, A. Montenero and G. Gnappi, *J. Electron Spectrosc. Related Phenom.*, 1998, **95**, 61;
- 30 C. Battistoni, M. P. Casaletto, G. M. Ingo, S. Kaciulis, G. Mattogno and L. Pandolfi, *Surf. Interface Anal.*, 2000, **29**, 773;
- 31 S. J. Bull, *Tribol. Int.*, 1997, **30**, 491;
- 32 C. Yang, T. Lui and L. Chen, *Thin Solid Films*, 2009, **517**, 5380;
- 33 R. A. Surmenev, *Surf. Coat. Tech.*, 2012, **206**, 2035;
- 34 B. León and J. Jansen, *Thin Calcium Phosphate Coatings for Medical Implants*, 2012, ISBN 978-0-387-77719-1;
- 35 A. R. Boyd, G. A. Burke, H. Duffy, M. Holmberg, C. O' Kane, B. J. Meenan and P. J. Kingshott, *Mater. Sci. Mater. Med.*, 2011, **22**, 71;
- 36 G. P. Dinda and J. Shin, J. Mazumder, *Acta Biomater.*, 2009, **5**, 1821;
- 37 A. Klymov, L. Prodanov, E. Lamers, J. A. Jansen and F. Walboomers, *Biomater. Sci.*, 2013, **1**, 135;
- 38 K. Anselme and M. Bigerelle, *Mater. Rev.*, 2001, **56**, 243;
- 39 H. Awaji, T. Matsunaga and S. Choi, *Mater. Trans.*, 2006, **47**, 1532;
- 40 A. Leyland and A. Matthews, *Wear*, 2000, **246**, 1;
- 41 M. A. Surmeneva, R. A. Surmenev, A. I. Tyurin, T. M. Mukhametkaliyev, A. D. Teresov, N. N. Koval, T. S. Pirozhkova, I. A. Shuvarin and C. Oehr, *Thin Solid Films*, 2014, **571**, 218;
- 42 K. A. Gross, S. Saber-Samandari and K. S. Heemann, *J. Biomed. Mater. Res. B Appl. Biomater.*, 2010, **93**, 1;
- 43 M. Roy, V. K. Balla, A. Bandyopadhyay and S. Bose, *Acta Biomater.*, 2011, **7**, 866;
- 44 K. A. Gross and S. Saber-Samandari, *Surf. Coat. Tech.*, 2009, **203**, 2995;
- 45 L. Latka, L. Pawlosski, D. Chicot, C. Pierlot and F. Petit, *Surf. Coat. Tech.*, 2010, **205**, 954;
- 46 H. Pelletier, A. Carradò, J. Faerber and I. N. Mihailescu, *Appl. Phys. A Mater. Sci. Proc.*, 2011, **102**, 629;
- 47 V. F. Pichugin, R. A. Surmenev, E. V. Shesterikov, M. A. Ryabtseva, E. V. Eshenko, S. I. Tverdokhlebov, O. Prymak and M. Epple, *Surf. Coat. Tech.*, 2008, **202**, 3913;
- 48 C. M. Cotell, D. B. Chrisey, K. S. Grabowski, J. A. Sprague and C. R. Gossett, *J. Appl. Biomater.*, 1992, **3**, 87.



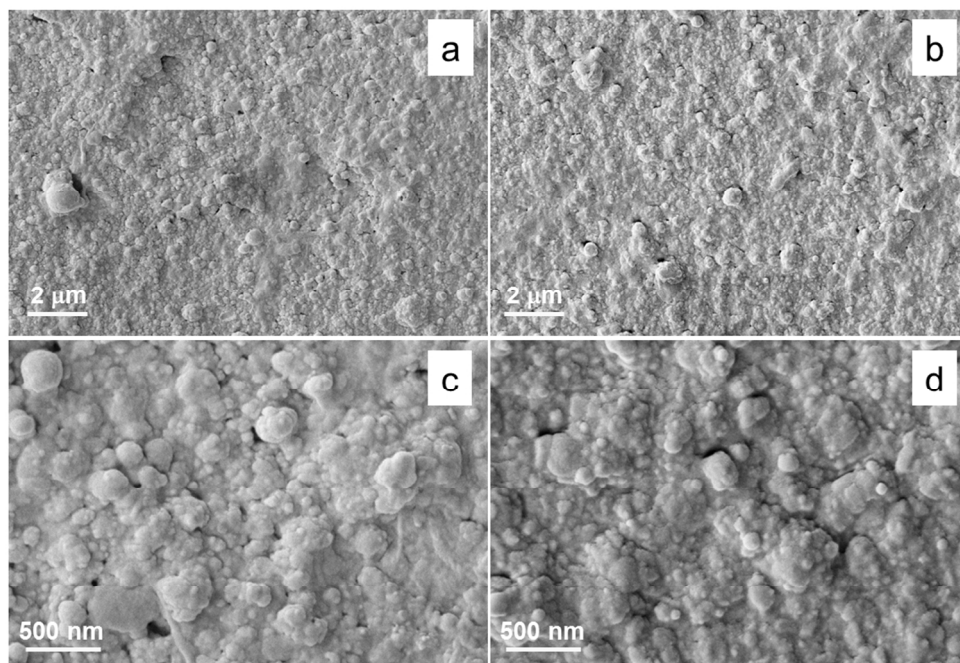
Sketch the Pulsed Plasma Deposition (PPD) system setup.  
226x167mm (150 x 150 DPI)



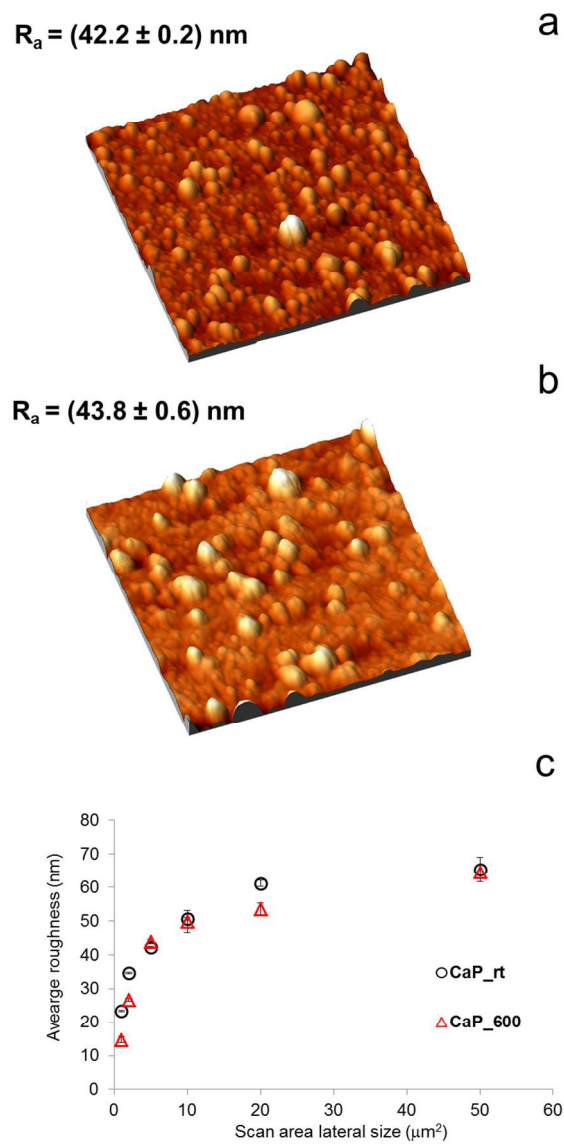
a) XRD patterns of as-deposited (i) and annealed (ii) CaP films. Curves are shifted for clarity. Curve in a) has been magnified 50 times. b) FTIR spectra of as-deposited (i) and annealed (ii) CaP films.  
206x284mm (150 x 150 DPI)



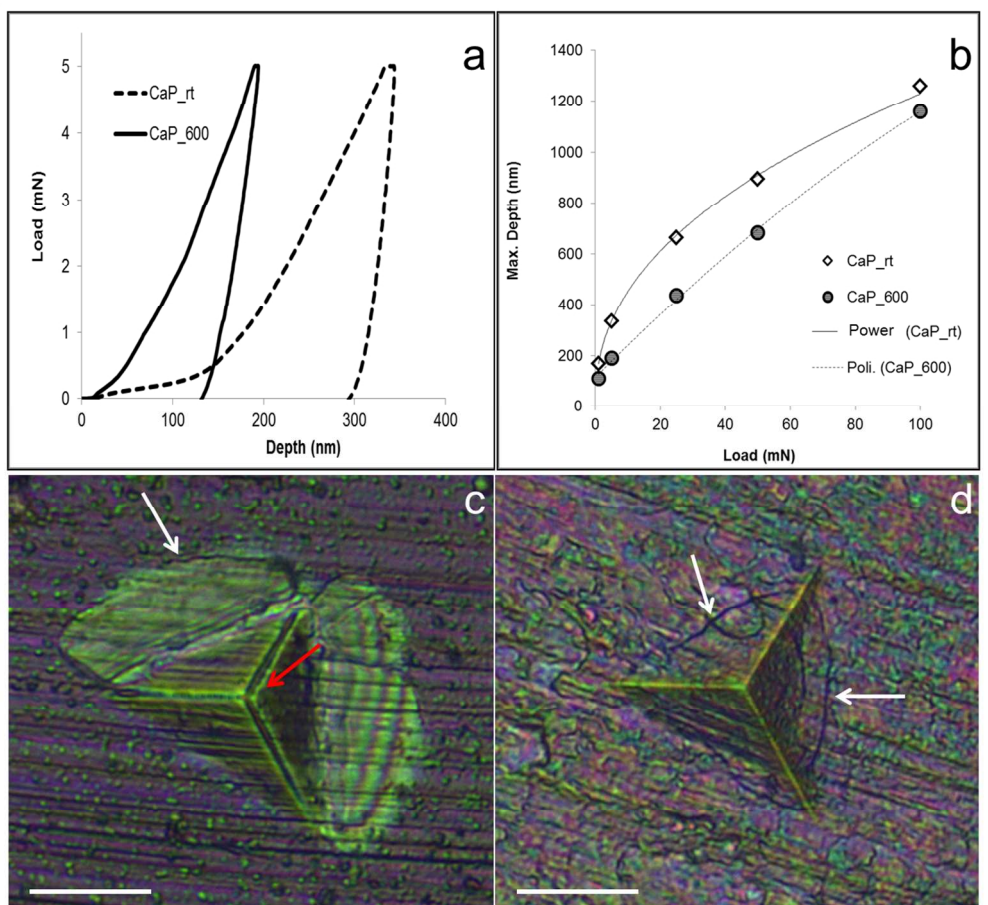
Deconvolution of XPS spectra acquired for the sample CaP<sub>rt</sub> sputtered for 300 s: a) Ca 2p region, b) O 1s region; c) XPS depth profile of the sample CaP<sub>rt</sub>.  
102x198mm (150 x 150 DPI)



FEG-SEM micrographs of CaP<sub>rt</sub> (a, c) and CaP<sub>600</sub> (b, d) at 25k (a, b) and 100k magnification (c, d).  
200x138mm (150 x 150 DPI)

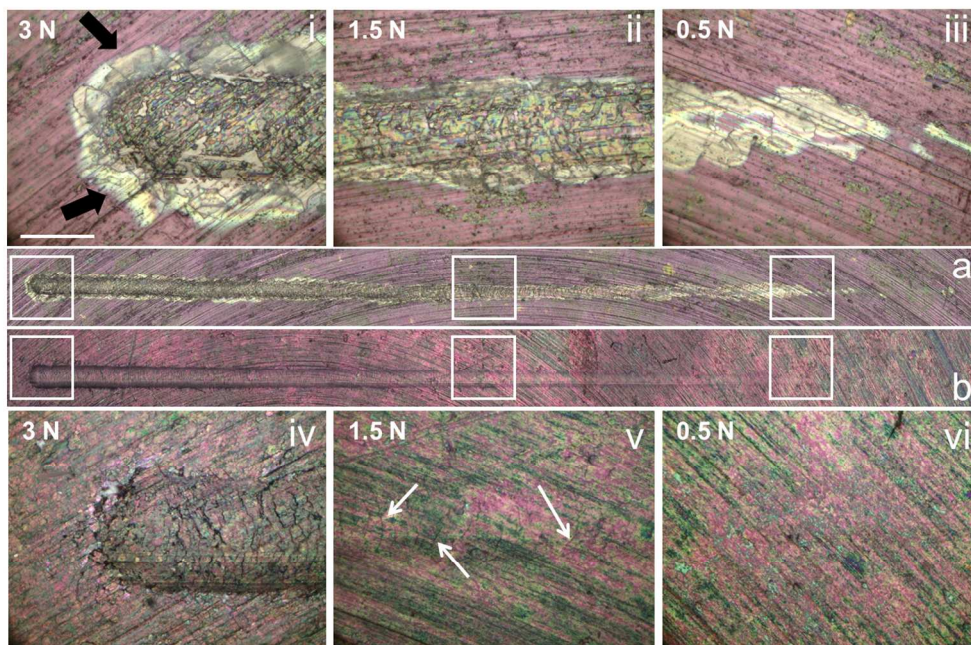


AFM 3D topographical images ( $5 \times 5 \mu\text{m}^2$ ) of CaP\_rt (a) and CaP\_600\_rt (b). In c), the average roughness of as-deposited and annealed films vs. the lateral size  $162 \times 294 \text{ mm}$  ( $150 \times 150 \text{ DPI}$ )

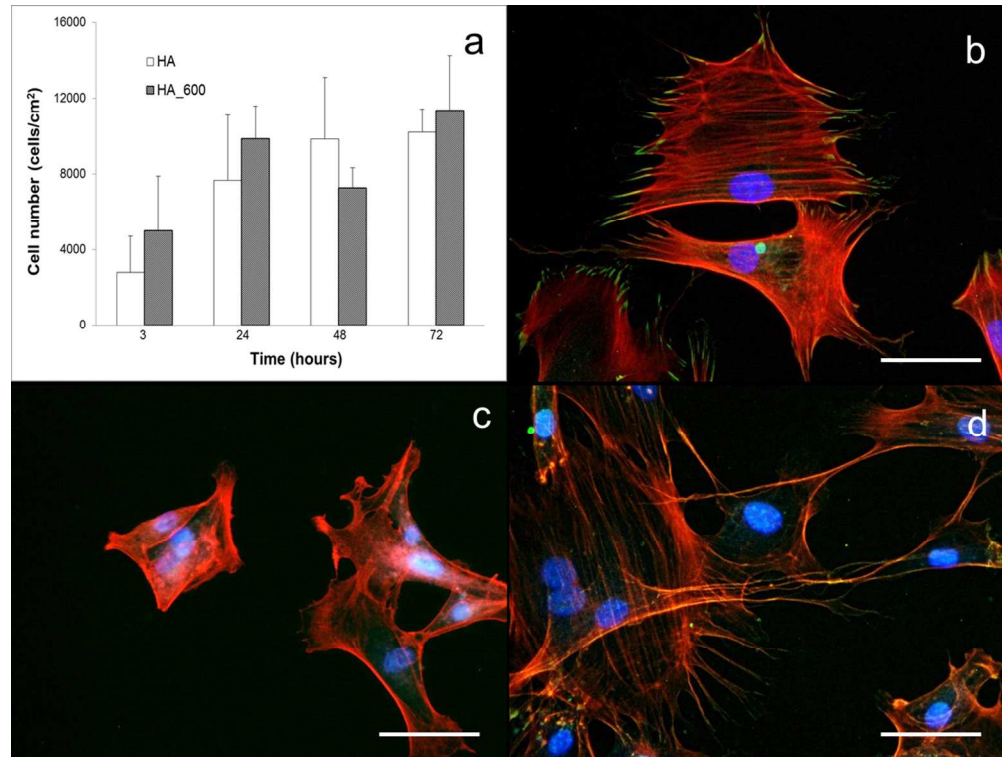


Panel showing the results of nanoindentation tests. In a) the mean load-depth curves of CaP<sub>rt</sub> and CaP<sub>600</sub> are reported for a maximum applied load of 5 mN. In b) the penetration depth achieved by the indenter tip for different loads ranging from 1 to 100 mN is reported, together with the relative curve fits. In c) and d), the indenter footprints left by a 500 mN load on as-deposited and annealed HA-coated titanium respectively, are shown (scale bar is 10  $\mu$ m). In c), white and red arrows mark the formation of pile-up and film detachment phenomena, respectively; in d), white arrows indicate the presence of internal film fractures, whilst radial cracks are not visible.

225x204mm (150 x 150 DPI)



Panel showing the worn tracks resulting from micro-scratch tests carried out imposing an increasing load from 0.1 to 3N on CaP<sub>rt</sub> (a) and CaP<sub>600</sub> (b). The inset i), ii), iii) are enlargements of the white squares of a), whereas iv), v) and vi) are enlargements of the white squares in b). Black arrows in i) indicate the wedging/spallation phenomenon. White arrows in v) indicate the presence of ductile tensile crackings.  
257x172mm (150 x 150 DPI)



Results of the in vitro cell tests. Osteoblasts cell number at 3, 24, 48 and 72h from seeding on CaP\_rt and CaP\_600 a). Immunostaining images evidencing the nuclei (DAPI, blue), the cytoskeleton (TRITC-conjugated Phalloidin, staining F-actin, red) and the focal adhesion point (FITC-anti-mouse IgG antibody, staining vinculin, green) of the cells at 3h (b, CaP\_600), 24h (c, CaP\_rt) and 72h (d, CaP\_600). The scale bar in b-d) is 50 μm.

219x164mm (150 x 150 DPI)

**Chemical composition in at. % and BE (eV)**

<i>Sample</i>	<i>O 1s</i>	<i>Ca 2p<sub>3/2</sub></i>	<i>P 2p</i>	<i>Ca/P</i>
<b>CaP_rt</b>	60.4 (530.7)	23.4 (347.8)	16.2 (133.8)	1.44
<b>CaP_600</b>	51.5 (531.3)	20.3 (347.7)	10.3 (133.8)	1.97

Chemical composition and Ca/P ratio of as-deposited and annealed films evaluated by XPS measurements.  
112x30mm (150 x 150 DPI)

## Nanoindentation test

---

<b>Sample</b>	<i>Hit (GPa)</i>	<i>Eit (GPa)</i>	<i>H/E</i>	<i>H<sup>3</sup>/E<sup>2</sup> (GPa)</i>
<b>CaP_rt</b>	4.2 ± 0.6	121 ± 23	0,035	5.1 x 10 <sup>-3</sup>
<b>CaP_600</b>	6.5 ± 0.5	108 ± 1	0,060	18.1 x 10 <sup>-3</sup>

Indentation hardness (HIT), elastic modulus (EIT), elastic strain to failure (H/E) and plastic deformation resistance (H<sup>3</sup>/E<sup>2</sup>) values for as-deposited and annealed films.  
138x82mm (150 x 150 DPI)